

# Transient Hydromagnetic Stagnation-Point Flow across a Vertical Surface with Partial Slip in a Chemically Reactive Medium

Shaban Museh<sup>1\*</sup>, Ibrahim Yakubu Seini<sup>2</sup>

<sup>1</sup>Mathematics Department, Gambaga College of Education, Gambaga, Ghana

<sup>2</sup>School of Engineering, University for Development Studies, Tamale, Ghana

Email: \*shabanmuseh@gmail.com, yakubuseini@yahoo.com

**How to cite this paper:** Museh, S. and Seini, I.Y. (2022) Transient Hydromagnetic Stagnation-Point Flow across a Vertical Surface with Partial Slip in a Chemically Reactive Medium. *Journal of Applied Mathematics and Physics*, **10**, 270-288.  
<https://doi.org/10.4236/jamp.2022.102021>

**Received:** December 8, 2021

**Accepted:** February 8, 2022

**Published:** February 11, 2022

Copyright © 2022 by author(s) and Scientific Research Publishing Inc.

This work is licensed under the Creative Commons Attribution International License (CC BY 4.0).

<http://creativecommons.org/licenses/by/4.0/>



Open Access

## Abstract

A numerical study of partial slip boundary condition is investigated. The stagnation-point flow problem involving some physio-chemical parameters has been elucidated. The process involves developing a multivariate mathematical model for the flow and transforming it into a coupled univariate equation. Key parameters of interest in the study are the buoyancy force, the surface stretching, the unsteadiness, the radiation, the dissipation effects, the slip effects, the species reaction and the magnetic field parameters. It is concluded that the impact of physio-chemical factors significantly alters the kinematics of the flow in order to optimally achieve desired product characteristics.

## Keywords

Transient Flow, Stagnation-Point, Partial Slip, Heat Transfer, Viscosity, Incompressible Fluid

## 1. Introduction

Heat and its transfer are major factors in every industrial process such as; chemical and process industries, mechanical and power generation plants, nuclear processes and thermal systems. Thermal plants are important in power generation to meet the energy requirements of modern industrial operations. With boilers and condensers operating in ways to achieve the desired rate of heat transfer, it is significant to consider factors that impact the design of electronic components to prevent system failure due to overheating. Using cast-iron and fabrication of semi-conductor components require uniform cooling [1]. The numerous applications of heat transfer in thermodynamics, diffusion theory,

material science, fluid dynamics, and the theory of radiation have made heat transfer the “heart” of thermal science.

Unsteady flow processes are common in nature and constitute majority of all flow in heat transfer phenomena. The effects of MHD in convective heat transfer across moving surfaces occur in many practical applications. Chamkha [2] employed the two-term functions in the forms of harmonic and non-harmonic to analyse the problem and observed that the solutal Grashof numbers enhanced the species concentration resulting in increased momentum. He further observed a decreasing rate of heat lost when the heat absorption parameter was increased and the mass transfer rate decreased with increasing Schmidt numbers. The unsteady boundary layer near stagnation points [3] [4] on stretched surfaces has extensively been reported. The heat transfer through vertical surfaces under convective heating [5] supports the findings that the wall surface friction and the mass transfer rate rise with the strength of the magnetic field as well as the convective heat exchange parameters.

Magnetic field has long been noted to have a great influence on boundary layer flow on porous surfaces and more so with chemically reactive flows. A study by [6] [7] examined the problem using perturbation techniques. Wang [8] [9] solved the Navier-Stokes equations and obtained dual solutions due to a stretched with partial slip conditions. Seini [10] extended the problem to include unsteadiness during the stretching in a chemically reacting medium that included a non-uniform source of heating. Similarly, surfaces that experience exponential stretching in conditions of thermal radiation and chemical reaction [11] have been reported.

Stagnation point flow is of great importance in process industries as its applications in polymer processing are enormous. It is also encountered in glass blowing, cooling of nuclear reactants and in harvesting of solar energy [12]. Partial slip has effects on transient hydromagnetic mixed convection flow [13] [14] [15] towards stagnation-points of shrinking surfaces. The effects of nonlinear [16] [17] shrinking towards stagnation points with slip and in micropolar fluid [18] [19] [20] [21] with slip boundary conditions have been widely reported.

This study investigates the transient hydromagnetic flow toward a vertical surface with partial-slip conditions prevailing within a chemically reactive medium. The rest of the manuscript is organized into the following sections: Section 2 describes the mathematical model along with the boundary conditions and the necessary assumptions. Section 3 outlined the numerical procedure whilst Section 4 reports on both the graphical and numerical results. Section 5 then outlined the conclusions and recommendations from the study.

## 2. The Mathematical Model

Consider a 2-D viscous flow of unsteady, incompressible, dissipative fluid towards a vertically stretched surface. Assuming the  $x$ - and  $y$ -axes are directed along the flow axis and normal to it respectively and a magnet with field of

strength  $B$  transversely applied in the direction of  $y$  positive. Assuming the plate is being stretched with a velocity that is proportional to the distance along the flow ( $x$ ) such that  $U_s = ax(1-ct)^{-1}$  with  $c$  representing the unsteadiness in the flow and  $a$  being a constant.  $a > 0$  represents a stretching surface whilst  $a < 0$  represents the shrinking surface.

The velocity of flow at the free stream is expressed as  $U_\infty = bx(1-ct)^{-1}$  with  $b > 0$  representing the strength of the stagnation flow. Furthermore, the stretched surface has a temperature of  $T_s$  related to the flow distance ( $x$ ), and time ( $t$ ) of flow as  $T_s = T_\infty + T_0x(1-ct)^{-2}$ .  $T_\infty$  denotes the temperature of the far distant streams, and a reference temperature  $T_0 \geq 0$ . Similarly, the stretching surface concentration  $C_s$  relates to the distance of flow ( $x$ ) and time ( $t$ ) as  $C_s = C_\infty + C_0x/(1-ct)^2$ , with  $C_\infty$  being the concentration at free stream and a reference concentration of  $C_0 \geq 0$  (Figure 1).

Expressions for  $U_s$ ,  $U_\infty$ ,  $T_s$  and  $C_s$  have been carefully chosen to allow for possible transformation of the modelled governing equations in partial form to linear ordinary differential equations. It has been noted that the expressions chosen are effective when time  $t < c^{-1}$  with  $a$ ,  $b$ , and  $c$ , having dimensions of per-second ( $s^{-1}$ ). Taking  $u$  and  $v$  to be the components of velocity in the flow direction of  $x$  and perpendicular direction of  $y$  respectively,  $T$  and  $C$  being the temperature and chemical species concentration fields respectively, the governing equations of the flow is obtained as:

$$\frac{\partial u}{\partial x} + \frac{\partial v}{\partial y} = 0, \tag{1}$$

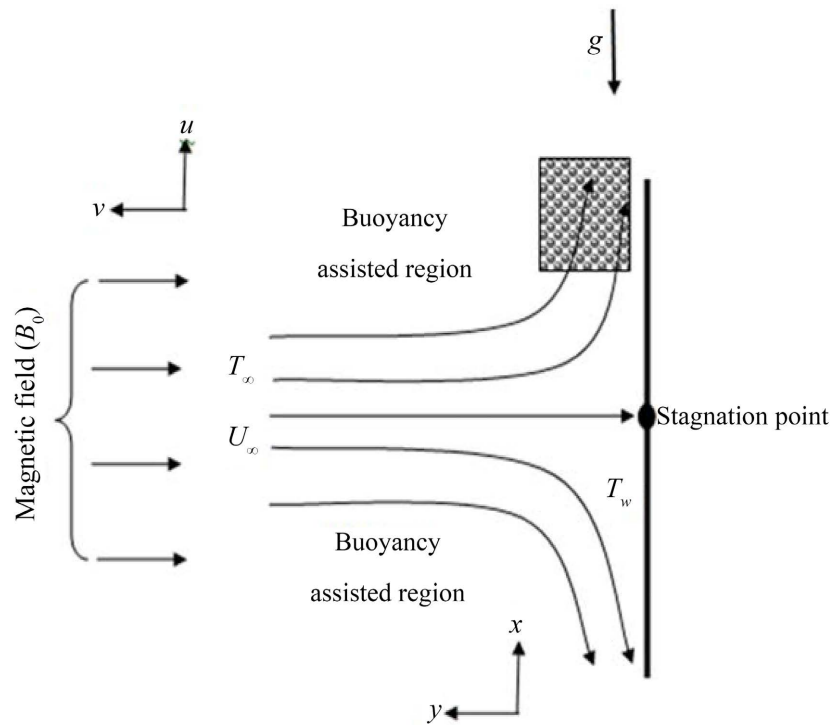


Figure 1. Schematic representation of the flow problem.

$$\frac{\partial u}{\partial t} + u \frac{\partial u}{\partial x} + v \frac{\partial u}{\partial y} = \frac{\partial U_\infty}{\partial t} + U_\infty \frac{\partial U_\infty}{\partial x} + \nu \frac{\partial^2 u}{\partial y^2} + g\beta_t(T - T_\infty) + g\beta_c(C - C_\infty) - \frac{\sigma B^2}{\rho} u, \quad (2)$$

$$\frac{\partial T}{\partial t} + u \frac{\partial T}{\partial x} + v \frac{\partial T}{\partial y} = \alpha \frac{\partial^2 T}{\partial y^2} + \frac{\nu}{c_p} \left( \frac{\partial u}{\partial y} \right)^2 + \frac{\sigma B^2}{\rho c_p} u^2 - \frac{\alpha}{\kappa} \frac{\partial q_r}{\partial y}, \quad (3)$$

$$\frac{\partial C}{\partial t} + u \frac{\partial C}{\partial x} + v \frac{\partial C}{\partial y} = D \frac{\partial^2 C}{\partial y^2} - \gamma(C - C_\infty) \quad (4)$$

where  $\nu$  is the fluid kinematic viscosity,  $g$  represents the acceleration due to gravity,  $D$  is the mass diffusivity,  $\beta_t$  is the thermal expansion coefficient,  $\beta_c$  is the solutal expansion coefficient,  $\gamma$  is the rate of chemical reaction,  $\kappa$  and  $\alpha$  represent the thermal conductivity coefficient and diffusivity respectively.

Expressions for the slip velocity ( $L$ ) and the solutal slip factor ( $N$ ) and the thermal slip factor ( $M$ ), are taken to be;  $L = l(1-ct)^{1/2}$ ,  $N = n(1-ct)^{1/2}$  and  $M = m(1-ct)^{1/2}$  with  $l$ ,  $n$  and  $m$  representing the initial slip-velocity, solutal-slip factor and the thermal-slip respectively. Noting these partial-slips, the boundary conditions are expressed in the form:

$$u = U_s + Lv \frac{\partial u}{\partial y}, \quad v = 0, \quad T = T_s + M \frac{\partial T}{\partial y}, \quad C = C_s + N \frac{\partial C}{\partial y} \quad \text{when } y = 0 \quad (5)$$

$$u \rightarrow U_\infty, \quad T \rightarrow T_\infty, \quad C \rightarrow C_\infty \quad \text{as } y \rightarrow \infty$$

Introducing the following dimensionless quantities:

$$\psi = x \sqrt{\frac{b\nu}{1-ct}} f(\eta), \quad \eta = y \sqrt{\frac{b}{(1-ct)\nu}}, \quad \theta = \frac{T - T_\infty}{T_s - T_\infty}, \quad \phi = \frac{C - C_\infty}{C_s - C_\infty} \quad (6)$$

Substituting Equation (6) into (1)-(5) yields:

$$f''' + f f'' - f'(f' + M) + Gt\theta + Gc\phi - A \left( \frac{\eta f''}{2} + f' - 1 \right) + 1 = 0 \quad (7)$$

$$\left( 1 + \frac{4}{3} Ra \right) \theta'' + Pr \left( f\theta' - f'\theta - \frac{A}{2} \eta \theta' - 2A\theta \right) + Br(Mf'^2 + f''^2) = 0 \quad (8)$$

$$\phi'' + Sc(f\phi' - f'\phi) - \frac{A}{2} Sc(\eta\phi' + 4\phi) - \beta Sc\phi = 0 \quad (9)$$

The boundary conditions are transformed to:

$$f(0) = 0, \quad f'(0) = \varepsilon + \delta f''(0), \quad \theta(0) = 1 + \zeta \theta', \quad \phi(0) = 1 + \xi \phi', \quad (10)$$

$$f'(\infty) \rightarrow 1, \quad \theta(\infty) \rightarrow 0, \quad \phi(\infty) \rightarrow 0$$

The prime symbol represents the order of derivative for a given function w.r.t the dimensionless similarity variable ( $\eta$ ), whereby  $Pr = \frac{\nu}{\alpha}$  (Prandtl number),

$Gt = \frac{g\beta_t T_0}{b^2}$  (Thermal Grashof number),  $Gc = \frac{g\beta_c C_0}{b^2}$  (Solutal Grashof number),

$Ra = \frac{4\sigma^* T_\infty^3}{\kappa K'}$  (Thermal radiation parameter),  $M = \frac{\sigma B_0^2}{\rho b}$  (Magnetic parameter),

$Br = \frac{\mu U_\infty^2}{\kappa(T_w - T_\infty)}$  (Brinkmann number),  $A = \frac{c}{b}$  (Unsteadiness parameter)

meter),  $\varepsilon = \frac{a}{b}$  (Ratio of stretching to free stream velocity parameter),  $\delta = l\sqrt{bv}$  (Dimensionless slip-velocity parameter),  $\zeta = m\sqrt{\frac{b}{v}}$  (Dimensionless thermal-slip parameter),  $\xi = n\sqrt{\frac{b}{v}}$  (Dimensionless solutal-slip parameter),  $Sc = \frac{\nu}{D}$  (Schmidt number) and  $\beta = \frac{\gamma}{b}(1-ct)$  (Reaction rate parameter).

### 3. Numerical Procedure

The coupled ordinary differential equations given in (7)-(9) along with the transformed boundary conditions in (10) are solved using the fourth-order Runge-Kutta integration scheme along with standard Newton-Raphson shooting method. Let

$$f = x_1, \quad f' = x_2, \quad f'' = x_3, \quad \theta = x_4, \quad \theta' = x_5, \quad \phi = x_6, \quad \phi' = x_7 \quad (11)$$

Equations (7)-(9) are reduced to 1<sup>st</sup> order system:

$$\begin{aligned} f' &= x_1' = x_2, \quad f'' = x_2' = x_3, \\ f''' &= x_3' = -x_1x_3 + x_2^2 - G_Tx_4 - Gcx_6 + Mx_2 + \frac{A}{2}(\eta x_3 + 2x_2 - 2) - 1, \\ \theta' &= x_4' = x_5, \\ \theta'' &= x_5' = -1/\left(1 + \frac{4}{3}Ra\right)\left(Pr(x_1x_5 - x_2x_4) - \frac{A}{2}Pr(\eta x_5 + 4x_4) + BrMx_2^2 + Brx_3^2\right), \\ \phi' &= x_6' = x_7, \quad \phi'' = x_7' = -Sc(x_1x_7 - x_2x_6) + \frac{A}{2}Sc(\eta x_7 + 4x_6) - Sc\beta x_6. \end{aligned} \quad (12)$$

The boundary conditions are transformed as:

$$\begin{aligned} x_1(0) &= 0, \quad x_2(0) = \varepsilon + \delta x_3(0), \quad x_3(0) = s_1, \quad x_4(0) = 1 + \zeta x_5(0), \\ x_5(0) &= s_2, \quad x_6(0) = 1 + \zeta x_7(0), \quad x_7(0) = s_3, \quad x_2(\infty) = 1, \quad x_4(\infty) = 0, \\ x_6(\infty) &= 0. \end{aligned} \quad (13)$$

During the shooting process, the unspecified initial conditions given by  $s_1, s_2$  and  $s_3$ , (13) are presumed and Equation (12) numerically integrated as an initial valued problem. The presumed value is compared to the computed value to check its accuracy at the end point. Any difference that exists is used to improve the missing initial condition and the procedure is repeated.

A symbolic and computational scheme written in MAPLE 16 platform is used to obtained results for various controlling parameters. Selecting a step size of  $\Delta\eta = 0.001$  to satisfy convergence criteria of  $10^{-7}$ , the extreme value of  $\eta_\infty$  to each parameter is found when the value of the unidentified boundary settings at  $\eta_\infty = 0$  not altered to successful loop with error less than  $10^{-7}$ . During the numerical computations, the wall frictional coefficient, the Nusselt number and the Sherwood number, which are related to  $f''(0), -\theta'(0)$  and  $-\phi'(0)$  respectively were computed and tabulated for various controlling parameters.

## 4. Results

### 4.1. Validation of Results

A comparison of results was done with reported data in literature [22] [23] as given in **Table 1**. This serves as a means of validation of the results and the numerical procedure. With no chemical reactive species, magnetic field, radiation, and viscous dissipation, the present study is in perfect agreement with Chen [23]. The problem reduces to the case of Pal [22] when the chemical species concentration, radiation and slip conditions with magnetic field effects are neglected.

### 4.2. Numerical Results

**Table 2** depicts the numerical results for wall friction coefficient, Nusselt number and Sherwood number for selected Prandtl numbers ( $Pr$ ), magnetic parameter ( $M$ ), radiation parameter ( $Ra$ ), Brinkmann number ( $Br$ ), the Schmidt number ( $Sc$ ) and the reaction rate parameter ( $\beta$ ). It is noted that the coefficient of wall friction increases with the Brinkmann number ( $Br$ ) but decreases with Prandtl number ( $Pr$ ), slip velocity parameter ( $\delta$ ), unsteadiness parameter ( $\alpha$ ), thermal slip parameter ( $\zeta$ ), and velocity ratio parameter ( $\epsilon$ ).

Viscous dissipation tends to increase frictional effects on the surface whereas the combined effects of the differences in momentum and thermal diffusivities, the velocity upstream and at the plate surface, the unsteadiness in the flow, the slip associated with the velocity and thermal distribution in the fluid tends to minimize the frictional effects on the plate surface. It is further noted that the rate of heat transfer rises with the Prandtl number but declines with increasing  $M$ ,  $Ra$ ,  $\beta$ ,  $Br$  and  $Sc$ . Furthermore, values of  $\beta$ ,  $Br$ ,  $Ra$  and  $Sc$  tends to increase the rate of mass transfer due to the existence of chemical reactants, mass diffusion, viscous dissipation and radiation.

**Table 3** represents the numerical results for the wall surface friction coefficient, local Nusselt and local Sherwood numbers with different values of thermal Grashof number ( $Gt$ ), velocity slip parameter ( $\delta$ ), velocity ratio parameter ( $\epsilon$ ), solutal Grashof number ( $Gc$ ), unsteadiness parameter (A thermal slip parameter

**Table 1.**  $f''(0)$  and  $-\theta'(0)$  for different values of  $Pr$  when  $\delta = \zeta = \xi = \alpha = 0$  and  $Gt = 1$ .

| $Pr$  | Pal [22] |               | Chen [23] |               | Present Study |               |
|-------|----------|---------------|-----------|---------------|---------------|---------------|
|       | $f''(0)$ | $-\theta'(0)$ | $f''(0)$  | $-\theta'(0)$ | $f''(0)$      | $-\theta'(0)$ |
| 0.72  | 0.36449  | 1.09331       | 0.36449   | 1.09311       | 0.36449       | 1.09310       |
| 6.80  | 0.18042  | 3.28957       | 0.18042   | 3.28957       | 0.18042       | 3.28957       |
| 20.0  | 0.11750  | 5.62014       | 0.11750   | 5.62013       | 0.11750       | 5.62013       |
| 40.0  | 0.08724  | 7.93831       | 0.08724   | 7.93830       | 0.08724       | 7.93831       |
| 60.0  | 0.07284  | 9.71801       | 0.07284   | 9.71800       | 0.07284       | 9.71801       |
| 80.0  | 0.06394  | 11.21875      | 0.06394   | 11.21873      | 0.06394       | 11.21874      |
| 100.0 | 0.05773  | 12.54113      | 0.05773   | 12.54109      | 0.05773       | 12.54110      |

**Table 2.** Effects of Parameter on Skin friction coefficient, Nusselt and Sherwood numbers.

| $Pr$ | $M$ | $\beta$ | $Ra$ | $Br$ | $Sc$ | $f''(0)$  | $-\theta'(0)$ | $-\phi'(0)$ |
|------|-----|---------|------|------|------|-----------|---------------|-------------|
| 0.71 | 0.1 | 0.1     | 0.1  | 0.1  | 0.24 | -0.660201 | 0.832081      | 0.570152    |
| 4.00 |     |         |      |      |      | -0.645661 | 1.712742      | 0.568820    |
| 7.10 |     |         |      |      |      | -0.564162 | 2.138431      | 0.568551    |
|      | 1.0 |         |      |      |      | -0.259332 | 0.722481      | 0.513710    |
|      | 1.5 |         |      |      |      | -0.099211 | 0.680581      | 0.489054    |
|      |     | 1.0     |      |      |      | -0.656922 | 0.831622      | 0.701933    |
|      |     | 1.5     |      |      |      | -0.655474 | 0.831421      | 0.764533    |
|      |     |         | 1.0  |      |      | -0.666314 | 0.609231      | 0.570904    |
|      |     |         | 1.5  |      |      | -0.668371 | 0.545460      | 0.571171    |
|      |     |         |      | 1.0  |      | -0.664202 | 0.678151      | 0.570724    |
|      |     |         |      | 1.5  |      | -0.666441 | 0.591356      | 0.571032    |
|      |     |         |      |      | 1.78 | -0.642993 | 0.829775      | 1.347444    |
|      |     |         |      |      | 2.64 | -0.639821 | 0.829438      | 1.580501    |

**Table 3.** Results of skin friction coefficient, Nusselt and Sherwood numbers for various values of  $Gt, Gc, A, \varepsilon, \delta, \zeta$  and  $\xi$ .

| $Gt$ | $Gc$ | $A$ | $\varepsilon$ | $\delta$ | $\zeta$ | $\xi$ | $f''(0)$  | $-\theta'(0)$ | $-\phi'(0)$ |
|------|------|-----|---------------|----------|---------|-------|-----------|---------------|-------------|
| 0.1  | 0.1  | 0.1 | 0.5           | 0.1      | 0.1     | 0.1   | -0.660201 | 0.832080      | 0.570151    |
| 1.0  |      |     |               |          |         |       | -0.949920 | 0.855994      | 0.588104    |
| 1.5  |      |     |               |          |         |       | -1.103361 | 0.867082      | 0.597093    |
|      | 1.0  |     |               |          |         |       | -1.012021 | 0.863401      | 0.595314    |
|      | 1.5  |     |               |          |         |       | -1.196542 | 0.877171      | 0.607562    |
|      |      | 1.0 |               |          |         |       | -0.734188 | 1.175041      | 0.785714    |
|      |      | 1.5 |               |          |         |       | -0.771837 | 1.321113      | 0.881287    |
|      |      |     | 1.0           |          |         |       | -0.001981 | 0.937230      | 0.618841    |
|      |      |     | 1.5           |          |         |       | -0.753652 | 1.008681      | 0.661612    |
|      |      |     |               | 1.0      |         |       | -0.308219 | 0.894708      | 0.598023    |
|      |      |     |               | 1.5      |         |       | -0.236404 | 0.905560      | 0.603154    |
|      |      |     |               |          | 1.0     |       | -0.646221 | 0.471314      | 0.569271    |
|      |      |     |               |          | 1.5     |       | -0.642665 | 0.379912      | 0.569044    |
|      |      |     |               |          |         | 1.0   | -0.646370 | 0.830686      | 0.376354    |
|      |      |     |               |          |         | 1.5   | -0.642094 | 0.830261      | 0.316643    |

( $\zeta$ ) and solutal slip parameter ( $\xi$ ). It is clear that the wall surface friction rises with selected values of  $\delta, \zeta$  and  $\xi$  and falls when the values of  $Gt, Gc, A,$  and  $\varepsilon$  are increased.

The velocity, solutal and thermal-slip parameters tend to increase the local skin friction; whereas the buoyancy forces (due to thermal and solutal diffusion); the velocity difference between the freestream and the surface, the unsteadiness parameter tend to reduce the wall surface friction. Furthermore, the rate of mass transfer rises with increasing  $Gt$ ,  $Gc$ ,  $A$ ,  $\varepsilon$ , and  $\delta$  and decrease with increasing  $\zeta$  and  $\xi$ .

### 4.3. Graphical Results

Graphical results for velocity, temperature and concentration profiles for pertinent parameters of interest in presented and discussed in this section

#### 4.3.1. Velocity Profiles

The velocity profiles for varying controlling parameters are displayed in **Figures 2-6**. In **Figure 2**, a decrease is noticed in the velocity field is a result of the increasing strength of the magnetic field intensity ( $M$ ). This is due to the fact that increasing the magnetic field strength leads to increasing the induced Lorenz force which offers high resistance to the flow field.

It is noted in **Figure 3** and **Figure 4** that thermal and solutal Grashof numbers enhance the velocity boundary layer due to the induced buoyancy forces. Similarly, **Figure 5** and **Figure 6** show that the velocity ratio and the unsteadiness parameter thicken the velocity boundary layer for obvious reasons. An increased in velocity ratio meant an increased in the free stream velocity against the plate surface velocity leading to increasing thickness of the velocity boundary layer.

#### 4.3.2. Temperature Distribution

**Figures 7-16** depicts the impact of increasing the pertinent control parameters

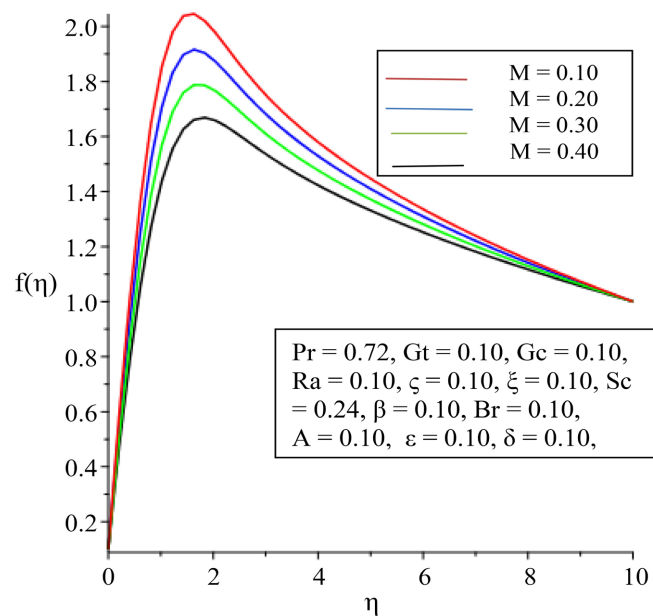


**Figure 2.** Effects of Velocity distribution with magnetic parameter ( $M$ ).

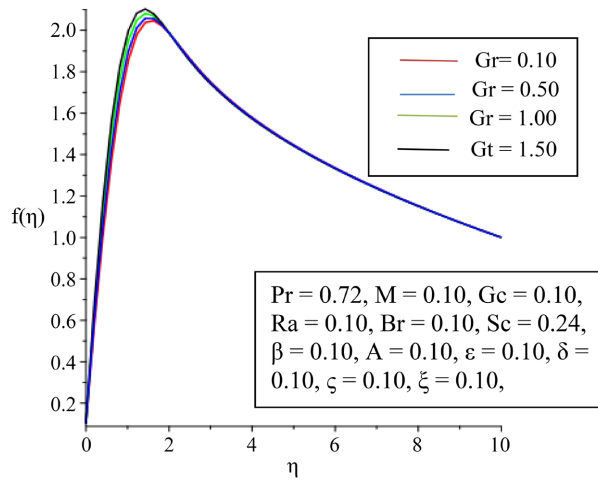


Figure 3. Effect of velocity distribution with thermal Grashof number ( $Gr$ ).

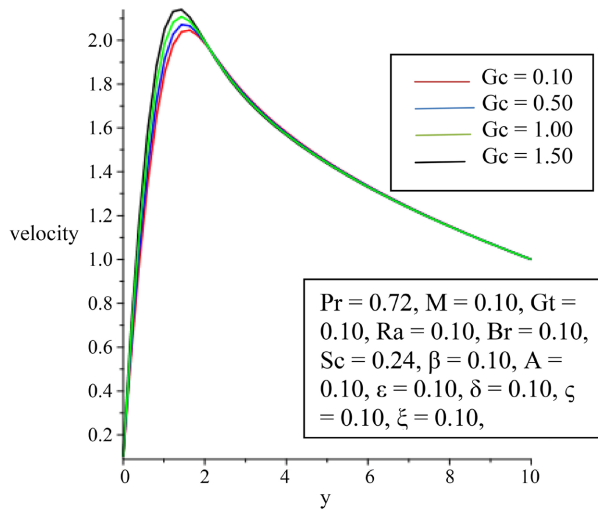


Figure 4. Effects of velocity distribution with Solutal Grashof number ( $Gc$ ).

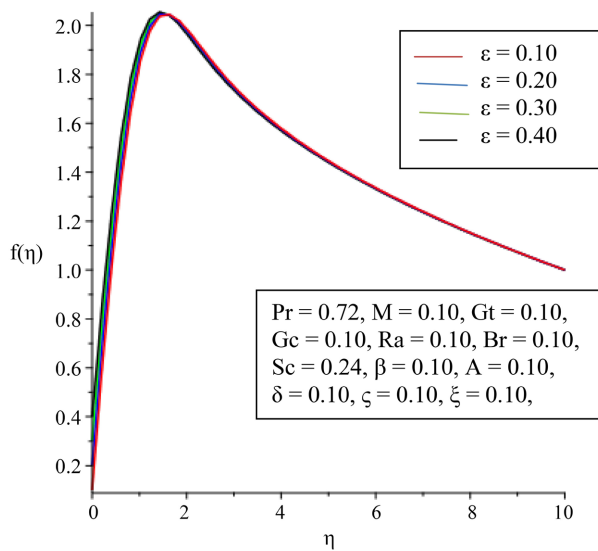
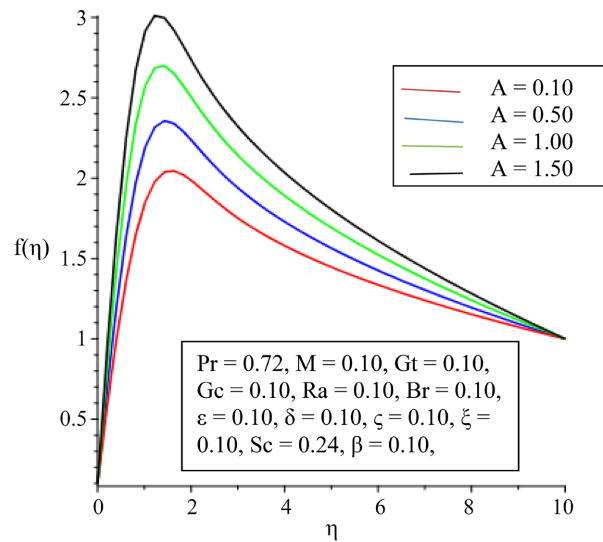
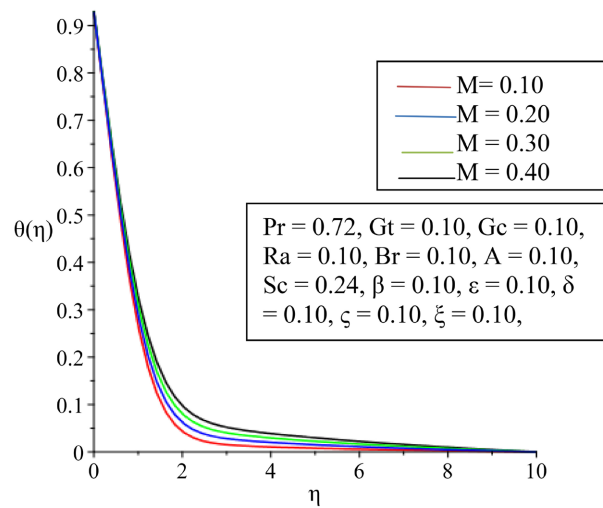


Figure 5. Effects of velocity distribution with velocity ratio parameter ( $\epsilon$ ).



**Figure 6.** Effects of velocity distribution with unsteadiness parameter ( $A$ ).



**Figure 7.** Temperature distribution for varying magnetic parameter ( $M$ ).

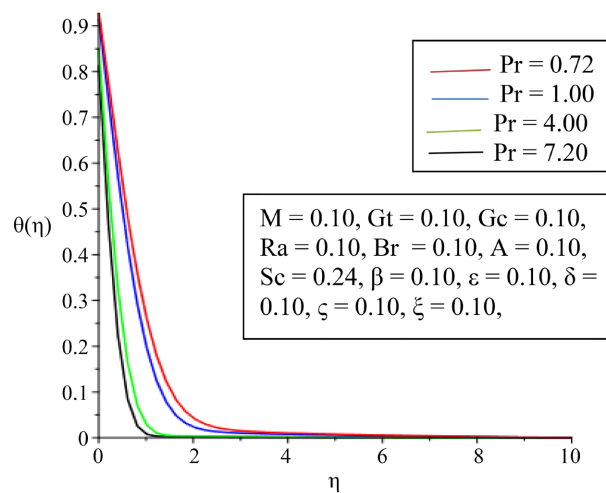


**Figure 8.** Temperature distribution for varying Prandtl number ( $Pr$ ).

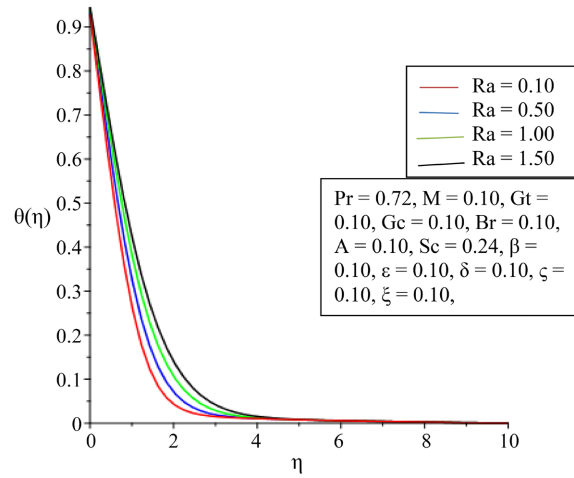


Figure 9. Temperature distribution for increasing radiation parameter ( $Ra$ ).

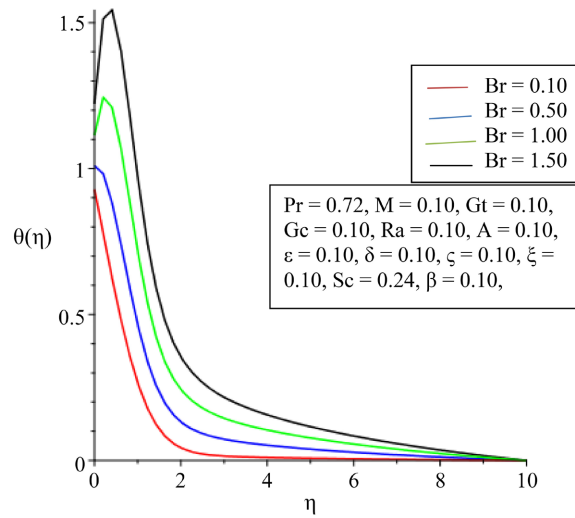


Figure 10. Temperature distribution for increasing Brinkmann number ( $Br$ ).

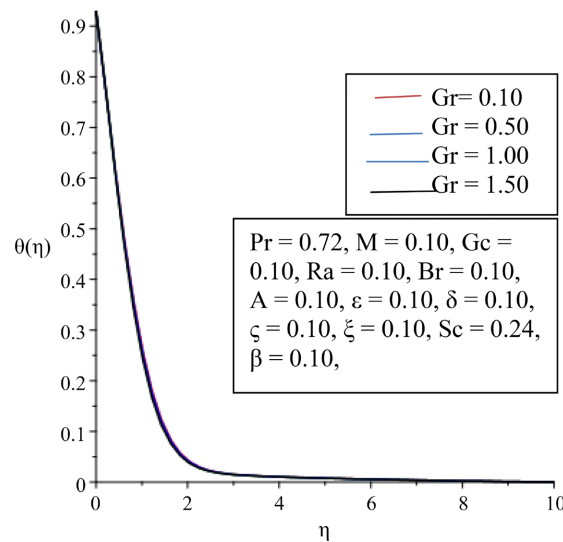
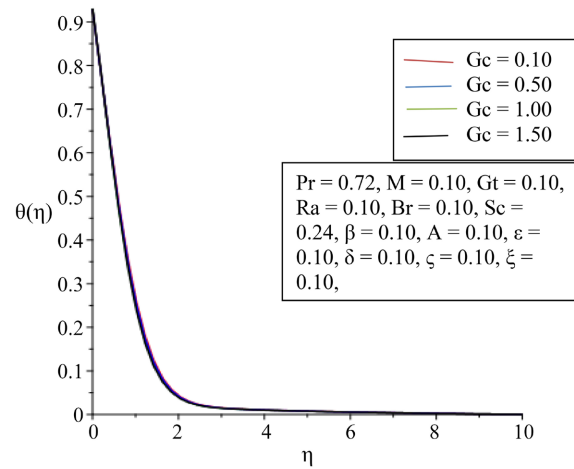
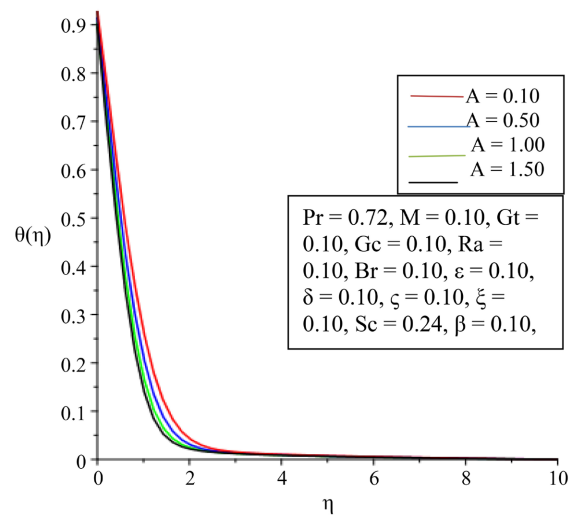


Figure 11. Temperature distribution for increasing thermal Grashof number ( $Gr$ ).



**Figure 12.** Temperature distribution for increasing solutal Grashof number ( $Gc$ ).



**Figure 13.** Temperature distribution for increasing unsteadiness Parameter ( $A$ ).

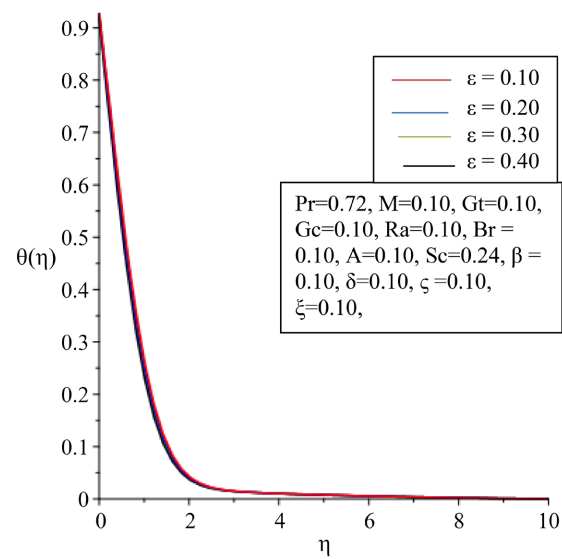


**Figure 14.** Temperature distribution for increasing velocity ratio parameter ( $\epsilon$ ).

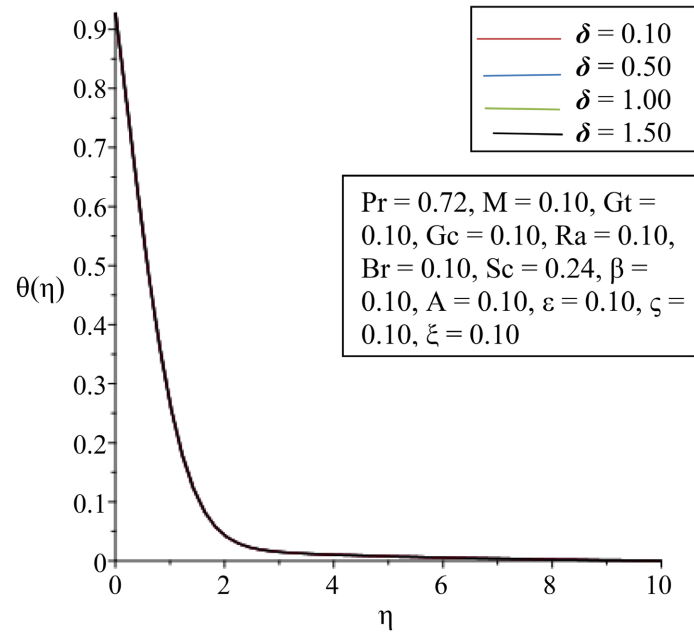


**Figure 15.** Temperature distribution for increasing velocity slip parameter ( $\delta$ ).

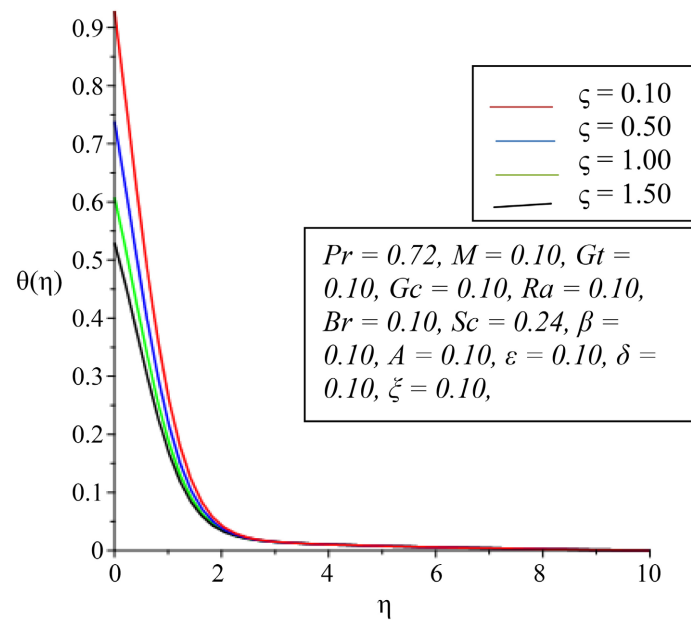


**Figure 16.** Temperature distribution for increasing thermal slip ratio ( $\zeta$ ).

on the flow. The intensity of the magnetic field tends to thicken the thermal boundary layer (Figure 7) due to the momentum reduction caused by the induced Lorenz force. This is often attributed to a situation known as Ohmic heating.

Prandtl number relates to the fluid viscosity and contributes to a reduction in the thermal boundary layer thickness (Figure 8). A high Prandtl number reduces the velocity field thereby lowering the thermal boundary layer thickness. Radiation from the surface leads to high molecular activity resulting in increased

temperature which then causes the thermal boundary layer thickness to increase (Figure 9). A similar trend is noticed with the Brinkmann number as the result of viscous dissipation.

Grashof numbers ( $Gt$  and  $Gc$ ) shown in Figure 11 and Figure 12 depicts a deteriorating temperature distribution caused by increased buoyancy forces. The unsteadiness parameter ( $A$ ) however leads to a diminishing thermal boundary layer (Figure 13).

Figures 14-16 depicts increasing thermal boundary layer when values of  $\varepsilon$ ,  $\delta$  and  $\zeta$  rise. This shows that the variance in velocity at free stream and on the surface, the slip velocity and slip associated with thermal distribution in the flow are to decrease the thermal boundary layer thickness near the bounding surface.

#### 4.3.3. Concentration Profiles

Figures 17-25 illustrate the impact of control parameters on species concentration within the boundary layer. The intensity of the magnetic field tends is seen to boost the species concentration near the bounding surface (Figure 17) whilst the reverse is observed for the rate of chemical reaction parameter depicted in Figure 18 and the Schmidt number shown in Figure 19) The observation is as a result of increasing Schmidt number which makes the momentum diffusivity to dominate the mass species diffusivity. Increasing reaction rate parameter indicates making the rate of chemical reaction higher than momentum leading to a reduction in the thickness of the concentration boundary layer. This is attributed to the case in which the reaction rate is of the destructive type and hence adversely impact on the species concentration.

Thermal buoyancy and solutal buoyancy parameters, Figure 20 and Figure 21 respectively, shows a reduction in the concentration of the chemical species. Similarly, Figures 22-25 show the impact of  $A$ ,  $\varepsilon$ ,  $\delta$  and  $\xi$  tend to diminish species concentration distribution near the surface for obvious reasons.

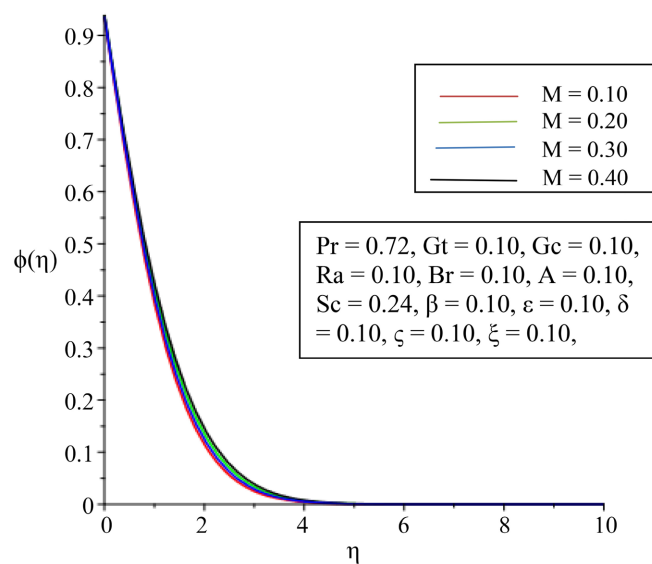


Figure 17. Concentration distribution for increasing magnetic parameter ( $M$ ).

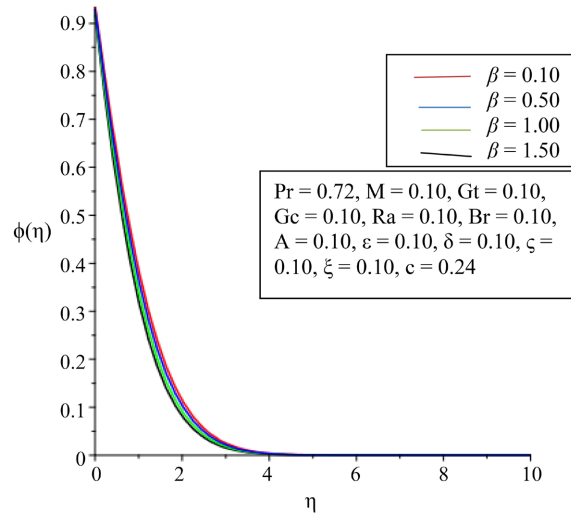


Figure 18. Concentration distribution for increasing reaction rate parameter ( $\beta$ ).

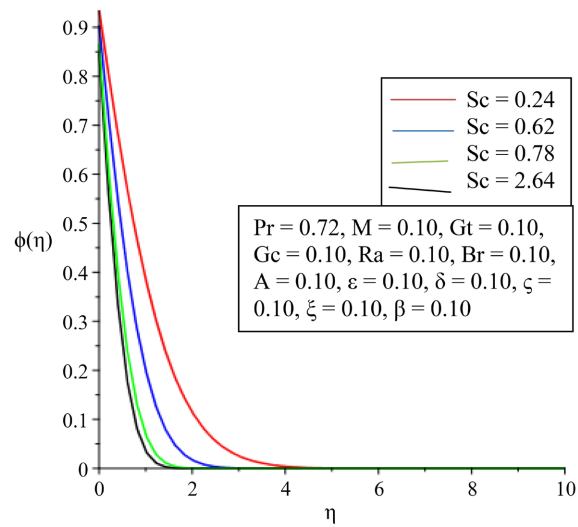


Figure 19. Concentration distribution for increasing Schmidt number ( $Sc$ ).

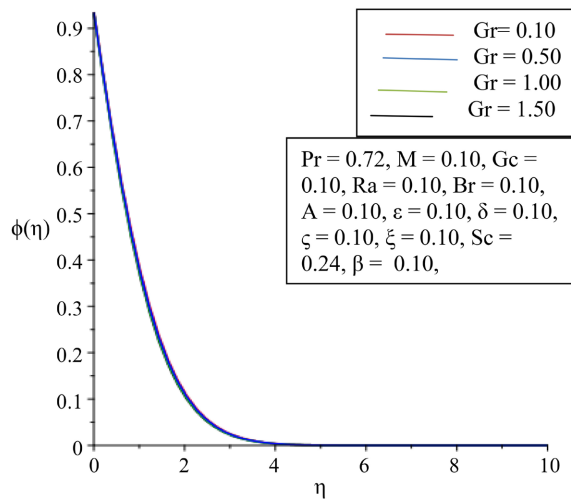
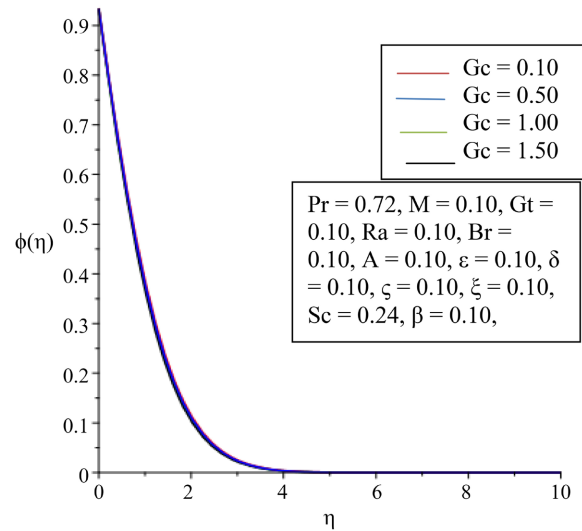
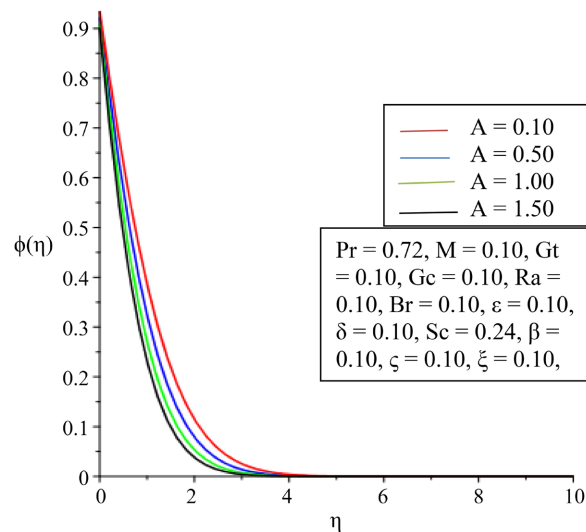


Figure 20. Concentration distribution for increasing thermal Grashof number ( $Gt$ ).



**Figure 21.** Concentration distribution for increasing Solutal Grashof number ( $Gc$ ).



**Figure 22.** Concentration distribution for increasing unsteadiness parameter ( $A$ ).

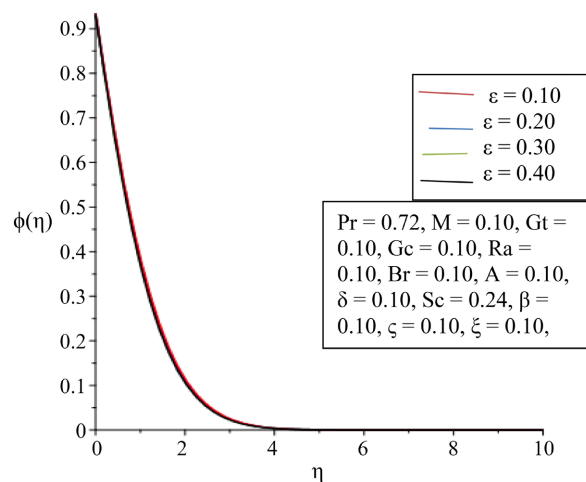


**Figure 23.** Concentration distribution for increasing velocity ratio parameter ( $\varepsilon$ ).

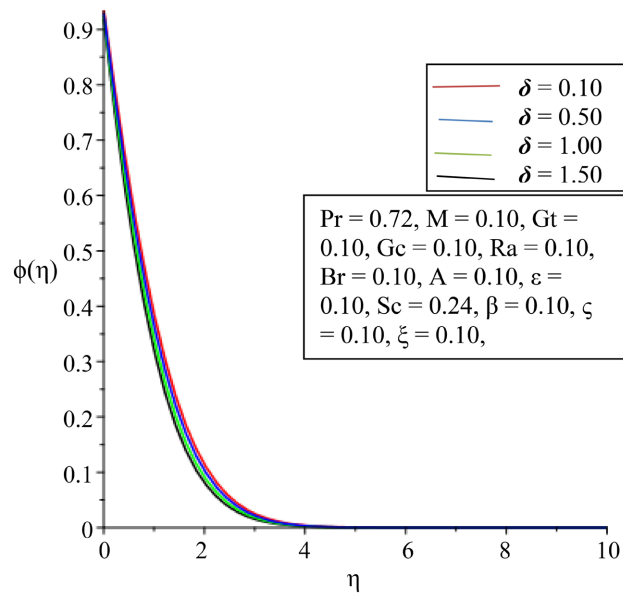


**Figure 24.** Concentration distribution for increasing velocity slip parameter ( $\delta$ ).

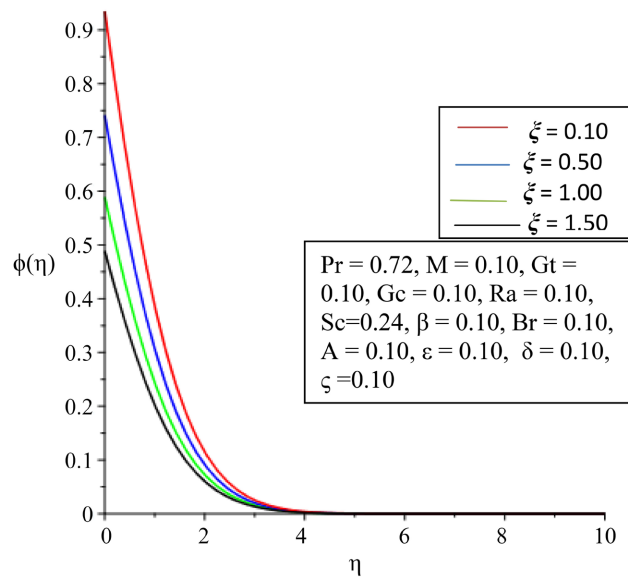


**Figure 25.** Concentration distribution for increasing solutal slip parameter ( $\xi$ ).

### 5. Conclusions

A transient hydromagnetic flow towards a stagnation point of vertical surface in the presence of viscous dissipation and radiation has been investigated with the following conclusions made:

- 1) The magnetic field parameter tends to decrease the velocity of the fluid thereby increasing the thermal and solutal boundary layer thicknesses due to the effects of the Lorenz forces induced by the magnetic field.
- 2) Both thermal and solutal Grashoh numbers have similar effects on the velocity profile with the solutal Grashof number showing move sensitivity to the flow but showing very slight variations within the thermal and concentration

boundary layers.

3) The unsteadiness of the flow and velocity ratio impact marginally on the flow. However, the unsteadiness significantly impedes the growth of the thermal boundary layer.

4) The solutal slip parameter has a pronounced effect on the concentration boundary layer particularly in the vicinity of the surface.

## Conflicts of Interest

The authors declare no conflicts of interest regarding the publication of this paper.

## References

- [1] Gupta, V. (2008) Heat and Mass Transfer. New Age International Publishers Limited, New Delhi, 396 p.
- [2] Chamkha, A.J. (2004) Unsteady MHD Convective Heat and Mass Transfer Past a Semi-Infinite Vertical Permeable Moving Plate with Heat Absorption. *International Journal of Engineering Science*, **42**, 217-230. [https://doi.org/10.1016/S0020-7225\(03\)00285-4](https://doi.org/10.1016/S0020-7225(03)00285-4)
- [3] Nazar, R., Amin, N., Filip, D. and Pop, I. (2004) Unsteady Boundary Layer Flow in the Region of the Stagnation Point on a Stretching Sheet. *International Journal of Engineering Science*, **42**, 1241-1253. <https://doi.org/10.1016/j.ijengsci.2003.12.002>
- [4] Sharma, P.R. and Singh, G. (2008) Unsteady Flow about a Stagnation Point on a Stretching Sheet in the Presence of Variable Free Stream. *Thammasat International Journal of Science and Technology*, **13**, 11-16.
- [5] Makinde, O.D. (2010) On MHD Heat and Mass Transfer over a Moving Vertical Plate with a Convective Surface Boundary Condition. *The Canadian Journal of Chemical Engineering*, **88**, 983-990. <https://doi.org/10.1002/cjce.20369>
- [6] Ibrahim, S.Y. and Makinde, O.D. (2010) On MHD Boundary Layer Flow of Chemically Reacting Fluid with Heat and Mass Transfer Past a Stretching Sheet. *International Journal of Fluid Mechanics*, **2**, 123-132.
- [7] Abdelkhalek, M.M. (2008) Heat and Mass Transfer in MHD Free Convection from a Moving Permeable Vertical Surface by a Perturbation Technique. *Communications in Nonlinear Science and Numerical Simulation*, **14**, 2091-2102. <https://doi.org/10.1016/j.cnsns.2008.06.001>
- [8] Wang, C.Y. (2002) Flow Due to a Stretching Boundary with Partial Slip—An Exact Solution of the Navier-Stokes Equations. *Chemical Engineering Science*, **57**, 3745-3747. [https://doi.org/10.1016/S0009-2509\(02\)00267-1](https://doi.org/10.1016/S0009-2509(02)00267-1)
- [9] Wang, C.Y. (2006) Stagnation Slip Flow and Heat Transfer on a Moving Plate. *Chemical Engineering Science*, **61**, 7668-7672. <https://doi.org/10.1016/j.ces.2006.09.003>
- [10] Seini, Y.I. (2013) Flow over Unsteady Stretching Surface with Chemical Reaction and Non-Uniform Heat Source. *Journal of Engineering and Manufacturing Technology*, **1**, 24-35.
- [11] Seini, Y.I. and Makinde, O.D. (2013) MHD Boundary Layer Flow Due to Exponential Stretching Surface with Radiation and Chemical Reaction. *Mathematical Problems in Engineering*, **2013**, Article ID: 163614. <https://doi.org/10.1155/2013/163614>
- [12] Arthur, E.M. and Seini, Y.I. (2014) MHD Thermal Stagnation Point Flow towards a

- Stretching Porous Surface. *Mathematical Theory and Modeling*, **4**, 163-169.
- [13] Aurang, Z., Bhattacharyya, K. and Shafie, S. (2016) Effect of Partial Slip on an Unsteady MHD Mixed Convection Stagnation-Point Flow of a Micropolar Fluid towards a Permeable Shrinking Sheet. *Alexandria Engineering Journal*, **55**, 1285-1293. <https://doi.org/10.1016/j.aej.2016.04.018>
- [14] Chiam, T.C. (1994) Stagnation-Point Flow towards a Stretching Plate. *Journal of the Physical Society of Japan*, **63**, 2443-2444.
- [15] Cao, K. and Baker, J. (2009) Slip Effects on Mixed Convective Flow and Heat Transfer from a Vertical Plate. *International Journal of Heat and Mass Transfer*, **52**, 3829-3841. <https://doi.org/10.1016/j.ijheatmasstransfer.2009.02.013>
- [16] Fauzi, N.F., Ahmad, S. and Pop, I. (2015) Stagnation Point Flow and Heat Transfer over a Nonlinear Shrinking Sheet with Slip Effects. *Alexandria Engineering Journal*, **54**, 929-934. <https://doi.org/10.1016/j.aej.2015.08.004>
- [17] Nik Long, N.M.A., Suali, M., Ishak, A., Bachok, N. and Arifin, N.M. (2016) Unsteady Stagnation Point Flow and Heat Transfer over a Stretching/Shrinking Sheet. *Journal of Applied Sciences*, **11**, 3520-3524. <https://doi.org/10.3923/jas.2011.3520.3524>
- [18] Mahapatra, T.R. and Nandy, S.K. (2016) Slip Effects on Unsteady Stagnation-Point Flow and Heat Transfer over a Shrinking Sheet. *Meccanica*, **48**, 1599-1606. <https://doi.org/10.1007/s11012-012-9688-1>
- [19] Soid, S.K., Ishak, A. and Pop, I. (2018) MHD Stagnation-Point Flow over a Stretching/Shrinking Sheet in a Micropolar Fluid with a Slip Boundary. *Sains Malaysia*, **47**, 2907-2916. <https://doi.org/10.17576/jsm-2018-4711-34>
- [20] Mohmood, K., Sajid, M., Ali, N. and Javed, T. (2018) Heat Transfer Analysis in the Time Dependent Axisymmetric Stagnation-Point Flow over a Lubricated Surface. *Thermal Science*, **22**, 2483-2492. <https://doi.org/10.2298/TSCI160203257M>
- [21] Adnan, N.S.M., Som, A.N.M., Arifin, N.M., Bachok, N., Ali, F.M. and Rahim, Y.F. (2020) A Stability Analysis of Boundary Layer Stagnation-Point Slip Flow and Heat Transfer towards a Shrinking/Stretching Cylinder over a Permeable Surface. *CFD Letters*, **12**, 97-105.
- [22] Pal, D. (2009) Heat and Mass Transfer in Stagnation-Point Flow towards a Stretching Surface in the Presence of Buoyancy Force and Thermal Radiation. *Meccanica*, **44**, 145-158. <https://doi.org/10.1007/s11012-008-9155-1>
- [23] Chen, H. (2014) Mixed Convection Unsteady Stagnation-Point Flow towards a Stretching Sheet with Slip Effects. *Mathematical Problems in Engineering*, **2014**, Article ID: 435697. <https://doi.org/10.1155/2014/435697>